Meshfree Methods Applied to Consolidation Problems in Saturated Soils

Pedro Navas, Susana López-Querol, Rena C. Yu and Bo Li

Abstract A meshfree numerical model, based on the principle of Local Maximum Entropy, with a B-Bar based algorithm to avoid instabilities, is applied to solve consolidation problems in saturated soils. This numerical scheme has been previously validated for purely elasticity problems without water (mono phase), as well as for steady seepage in elastic porous media. Hereinafter, the model is validated for well known consolidation theoretical problems, both static and dynamic, with known analytical solutions. For several examples, the solutions obtained with the new code are compared to PLAXIS (commercial software). Finally, after validated, solutions for dynamic radial consolidation and sinks, which have not been found in the literature, are presented as a novelty. This new numerical approach is demonstrated to be feasible for this kind of problems in porous media.

1 Introduction

The settlement of saturated soils under loading is caused by a gradual interchange between pore pressure and effective stress. Immediately after external loadings are applied to a saturated soil domain, all the external pressure transfers to water, and

P. Navas · R.C. Yu (✉)
School of Civil Engineering, University of Castilla La-Mancha, Avda. Camilo Jose Cela s/n, 13071 Ciudad Real, Spain
e-mail: pedro.navas@uclm.es

R.C. Yu
e-mail: rena@uclm.es

S. López-Querol
Department of Civil, Environmental and Geomatic Engineering, University College London, Gower Street, London WC1E 6BT, UK
e-mail: s.lopez-querol@ucl.ac.uk

B. Li
Department of Mechanical and Aerospace Engineering, Case Western Reserve University, Cleveland, OH 44106, USA
e-mail: bo.li4@case.edu

K. Weinberg and A. Pandolfi (eds.), *Innovative Numerical Approaches for Multi-Field and Multi-Scale Problems*, Lecture Notes in Applied and Computational Mechanics 81, DOI 10.1007/978-3-319-39022-2_11

some time is required for drainage to take place. When this drainage (i.e. dissipation of excess pore pressures) is complete, the solid phases totally takes the external pressure. This process is known as *soil consolidation* [1]. The implementation of the Biot's equations [2] is a well-known way to solve problems in porous media from a macro-scale point of view. The advantage of this method is the possibility of accounting for coupling between the fluid phase and the solid skeleton. The $u - p_w$ formulations, where u denotes the solid phase displacement, and p_w is the pore fluid pressure [3], have traditionally been employed for simulating coupled problems in saturated porous media since the final equations work with less degrees of freedom (three in 2D, four in 3D problems) compared with that of a complete formulation. The recent $u - w$ formulation, where w represents the relative fluid displacement with respect to the solid phase, which is usually referred as the displacement-based or complete formulation, has been employed in several numerical schemes (López-Querol et al. [4], and recently adopted by Cividini and Gioda [5]). Such a methodology is assumed in this work, first for its simplicity in imposing impervious boundary conditions compared to the $u - p_w$ approaches; second, as the free surface comes out naturally as the zero-pressure contour, no detection algorithm is necessary; third, it facilities the modelling of large and/or nonlinear deformations of the solid phase as well as the possible separation between the solid and fluid phases in the case of local failure (liquefaction or slope instability). Since meshfree numerical schemes have been known to perform particularly well in the regime of large deformations, we endeavour to apply such schemes to coupled problems in saturated porous media, using the $u - w$ formulation.

There are many different flavours of meshfree methods available. The present research has been carried out using the principle of maximum entropy [6], the shape functions developed by Arroyo and Ortiz [7], in particular, the OTM framework [8], for its numerous advantages in comparison with its alternatives. For example, the exact mass transport, the satisfaction of the continuity equation, exact linear and angular momentum conservation in order to solve different problems as spurious modes, tensile instabilities and unknown convergence or stability properties. Since the deformation and velocity fields are interpolated from nodal values using maxent shape functions, the Kronecker-delta property at the boundary makes it possible for the direct imposition of essential boundary conditions. In the current work, an Eulerian framework is employed to solve the Biot's equations for porous media. In addition, the parameters pertinent to the local maximum entropy are obtained efficiently and independent of the support size through the Nelder-Mead algorithm [9].

Locking in near-incompressible materials is not unusual for the numerical methods based on either finite elements approaches [10–17] or meshfree approximation schemes [18]. In the case of flow through saturated media, in a displacement formulation, since both the undrained soil phase and the fluid phase are nearly incompressible, locking may also occur. The recent approach developed by Ortiz and Sukumar [18], avoids locking by averaging the volumetric part of the strain tensor with the value of the pressure. However, since the pressure term is part of the constitutive model employed, the constitutive model is necessarily modified. As an alternative, we implement a volumetric-strain average instead of a pressure average approach.

The proposed algorithm is independent of the constitutive model employed and it is generically applicable to solve other locking problems. The idea behind is inspired by that of Hughes [10] and the posterior developments of the B-Bar method [16]. The specific strategy is analogous to that of the diamond elements of Hauret, Kuhl and Ortiz [15] and it is the first B-Bar implementation for a pure displacement approach within the framework of meshfree methods. It is also straightforward to be extended for finite deformations and nonlinear applications. Extension of the formulation by the authors in [19] to axisymmetric framework is presented in the current work.

The rest of the paper is organised as follows. The mathematical framework, including the B-Bar based algorithm is presented next. Applications to various consolidation problems are illustrated in Sect. 3. Relevant conclusions are drawn in Sect. 4.

2 Mathematical Framework

In this section, we first summarise the governing equations for unconfined seepage problems, in particular, the Biot's equations, formulated in a $u-w$ framework, which have been successfully utilised by López-Querol et al. [20, 21], Cividini and Gioda [5]; next, the B-bar implementation in axisymmetric framework for elastic and porous media are given in detail.

2.1 The Biot's Equations: A u − w Formulation

The Biot's equations [22] are based on formulating the mechanical behaviour of a solid-fluid mixture, the coupling between different phases, and the continuity of flux through a differential domain of saturated porous media. For clarity, bold symbols for notation of vectors and matrices, and regular letters to denote scalar variables, are used. Let ρ and ρ_f respectively represent the mixture and fluid phase densities; $\boldsymbol{b}$ and κ stand for the external acceleration vector and the permeability coefficient in [$m^3 \cdot$ s/kg] (in civil engineering, however, the notion of hydraulic conductivity, $k = \kappa \rho_f g$, in [m/s], is often used instead), the three equations of Biot, which represent the mixture equilibrium, the fluid phase equilibrium and the continuity equation respectively, are expressed as follows:

$$\boldsymbol{S}^T d\boldsymbol{\sigma} - \rho d\ddot{\boldsymbol{u}} - \rho_f d\ddot{\boldsymbol{w}} + \rho d\boldsymbol{b} = 0, \tag{1}$$

$$-\nabla dp_w - \kappa^{-1} d\dot{\boldsymbol{w}} - \rho_f d\ddot{\boldsymbol{u}} - \frac{\rho_f}{n} d\ddot{\boldsymbol{w}} + \rho_f d\boldsymbol{b} = 0, \tag{2}$$

$$\nabla \cdot d\dot{\boldsymbol{w}} + \boldsymbol{m} \cdot d\dot{\boldsymbol{\varepsilon}}^s + \frac{d\dot{p}_w}{Q} = 0, \tag{3}$$

where $\boldsymbol{S}$ is a differential operator, $\boldsymbol{u}$ is the displacement vector of the solid skeleton and $\boldsymbol{w}$ is the relative displacement of the fluid phase with respect to the solid one. By denoting $\boldsymbol{U}$ as the absolute displacement of the fluid phase, $\boldsymbol{w}$ is related with $\boldsymbol{U}$ through the soil porosity, n, as follows:

$$\boldsymbol{w} = n(\boldsymbol{U} - \boldsymbol{u}). \tag{4}$$

Additionally in Eq. (3), $\boldsymbol{m}$ represents the unit matrix expressed in Voigt form, whereas Q stands for the mixture compressibility, which is calculated as

$$Q = \left[K_s^{-1}(1-n) + nK_f^{-1}\right]^{-1}, \tag{5}$$

where K_s and K_f are the bulk modulus of the solid grains and the compressive modulus of the fluid phase.

A 2D approach is considered in the derivations presented hereinafter, therefore the differential operator, $\boldsymbol{S}$, and the unit matrix $\boldsymbol{m}$ are written as

$$\boldsymbol{S} = \begin{pmatrix} \frac{\partial}{\partial x} & 0 \\ 0 & \frac{\partial}{\partial y} \\ \frac{\partial}{\partial y} & \frac{\partial}{\partial x} \end{pmatrix}, \quad \boldsymbol{m} = \begin{pmatrix} 1 \\ 1 \\ 0 \end{pmatrix}. \tag{6}$$

Assuming tensile stresses (except pore pressure p_w, which is positive for compression) and strains as positive, the Terzaghi's effective stress [23] is defined as follows

$$\boldsymbol{\sigma} = \boldsymbol{\sigma'} - p_w \boldsymbol{m}, \tag{7}$$

where $\boldsymbol{\sigma'}$ and $\boldsymbol{\sigma}$ are the respective vectorial form in Voigt notation for the effective and total stress tensor. For the case of linear elasticity, the incremental relationship between stresses and strains is governed by:

$$\boldsymbol{d\sigma'} = \boldsymbol{D^e d\varepsilon^s}, \tag{8}$$

where $\boldsymbol{D^e}$ denotes the elastic tensor, which under plane strain conditions, it is given by:

$$\boldsymbol{D^e} = \frac{\lambda}{\nu} \begin{pmatrix} 1-\nu & \nu & 0 \\ \nu & 1-\nu & 0 \\ 0 & 0 & \frac{1-2\nu}{2} \end{pmatrix} \tag{9}$$

where ν is the Poisson's ratio, λ, the first constant of Lamé.

Rearranging the above equations, Eq. (1) can be re-written as

$$\boldsymbol{S^T D^e S du} - \nabla dp_w - \rho \boldsymbol{d\ddot{u}} - \rho_f \boldsymbol{d\ddot{w}} + \rho \boldsymbol{db} = 0. \tag{10}$$

In the $u-w$ approach, also known as the *complete* formulation (no additional assumption is required under plane strain conditions), each node has four degrees of freedom, $\boldsymbol{u}$ and $\boldsymbol{w}$ (two components each in 2D problems) and the scalar p_w, the pore pressure, is obtained afterwards. By comparison, in the traditional $u-p_w$ formulation, each node has only three degrees of freedom in 2D, but results in complications in imposing impervious boundary conditions.

Integrating Eq. (3) in time, and substituting dp_w in Eqs. (10) and (2), it yields:

$$\boldsymbol{S^T D^e S du} + Q\nabla\left(\nabla^T \boldsymbol{du}\right) + Q\nabla\left(\nabla^T \boldsymbol{dw}\right) - \rho \boldsymbol{d\ddot{u}} - \rho_f \boldsymbol{d\ddot{w}} + \rho \boldsymbol{db} = 0, \tag{11}$$

$$Q\nabla\left(\nabla^T \boldsymbol{du}\right) + Q\nabla\left(\nabla^T \boldsymbol{dw}\right) - k^{-1}\boldsymbol{d\dot{w}} - \rho_f \boldsymbol{d\ddot{u}} - \frac{\rho_f}{n}\boldsymbol{d\ddot{w}} + \rho_f \boldsymbol{db} = 0. \tag{12}$$

Note that an isotropic medium is assumed in the above equations. The final system of equations, once the elementary matrices have been assembled, can be expressed as:

$$\boldsymbol{Kdu} + \boldsymbol{C}\boldsymbol{d\dot{u}} + \boldsymbol{M}\boldsymbol{d\ddot{u}} = \boldsymbol{df}, \tag{13}$$

where $\boldsymbol{K}$, $\boldsymbol{C}$ and $\boldsymbol{M}$ respectively denote stiffness, damping and mass matrices, $\boldsymbol{du}$ represents the vector of unknowns (containing both the solid phase and fluid displacements, $\boldsymbol{u}$ and $\boldsymbol{w}$), expressed incrementally, and $\boldsymbol{df}$ is the increment of the external forces vector, containing gravity acceleration, as well as boundary conditions for nodal forces.

2.2 B-Bar Formulation in Elastic Axisymmetric Problems

In axisymmetric problems, x direction is changed by r, y changes to z. Due to this fact, the shape function based on the principle of Local Maximum Entropy is similar to that of the 2D case. Consequently, the new displacement vector is calculated with the following equation:

$$\begin{bmatrix} u_r \\ u_z \end{bmatrix} = \begin{bmatrix} N_1 & 0 & N_2 & 0 & \cdots \\ 0 & N_1 & 0 & N_2 & \cdots \end{bmatrix} \begin{bmatrix} u_{r1}^h \\ u_{z1}^h \\ u_{r2}^h \\ u_{z2}^h \\ \vdots \end{bmatrix}, \tag{14}$$

where the superscript ^{h} denotes discrete nodal values. In an axisymmetric problem, a different ε matrix is obtained according to [24]:

$$\begin{bmatrix} \varepsilon_r \\ \varepsilon_z \\ \varepsilon_\theta \\ \gamma_{rz} \end{bmatrix} = \begin{bmatrix} \frac{\partial}{\partial r} & 0 \\ 0 & \frac{\partial}{\partial z} \\ \frac{1}{r} & 0 \\ \frac{\partial}{\partial z} & \frac{\partial}{\partial r} \end{bmatrix} \begin{bmatrix} u_r \\ u_z \end{bmatrix}. \tag{15}$$

Voigt notation is assumed in order to obtain the final B-bar matrix. The process to obtain B matrix in index notation is:

$$\varepsilon_l = S_{lj} u_j = S_{lj} N_{jk} u_k^h = B_{lk} u_k^h.$$

Thereby, the B matrix is the following one:

$$\mathbf{B} = \left[\begin{array}{cc|cc|c} \frac{\partial N_1}{\partial r} & 0 & \frac{\partial N_2}{\partial r} & 0 & \\ 0 & \frac{\partial N_1}{\partial z} & 0 & \frac{\partial N_2}{\partial z} & \cdots \\ \frac{N_1}{r} & 0 & \frac{N_2}{r} & 0 & \\ \frac{\partial N_1}{\partial z} & \frac{\partial N_1}{\partial r} & \frac{\partial N_2}{\partial z} & \frac{\partial N_2}{\partial r} & \end{array}\right]. \tag{16}$$

If σ is required, the following equation should be employed:

$$\boldsymbol{\sigma} = \begin{bmatrix} \sigma_r \\ \sigma_z \\ \sigma_\theta \\ \tau_{rz} \end{bmatrix} = D\boldsymbol{\varepsilon}, \tag{17}$$

where

$$\boldsymbol{D} = \frac{\lambda}{\nu} \begin{bmatrix} 1-\nu & \nu & \nu & 0 \\ \nu & 1-\nu & \nu & 0 \\ \nu & \nu & 1-\nu & 0 \\ 0 & 0 & 0 & \frac{1-2\nu}{2} \end{bmatrix}. \tag{18}$$

Stiffness matrix is calculated by taking into account that the volume integral is extended around the whole ring of material as follows:

$$\mathbf{K^p} = 2\pi \int \mathbf{B^T D B}\, r\, dr\, dz, \tag{19}$$

where the superscript ^{p} represents the fact that the matrix is calculated for each material point within a patch. The final expression is written as:

$$\mathbf{K}^p = 2\pi \overline{\mathbf{B}}^{\mathbf{T}} \mathbf{D} \overline{\mathbf{B}}\, \bar{r} A, \tag{20}$$

where A is the associated area of the material point.

The external forces in Eq. (13) are calculated in the same way:

$$\mathbf{f} = \begin{bmatrix} 2\pi r f_r \\ 2\pi r f_z \end{bmatrix}, \tag{21}$$

where f_r and f_z respectively denote radial and vertical components of the external force.

If a B-Bar based algorithm is implemented in this problem, the starting point is similar to the plane strain one, which is based on the transformation of the $\boldsymbol{\varepsilon}$ tensor to the $\overline{\boldsymbol{\varepsilon}}$ tensor, a tensor where the volumetric part is obtained as an average of the neighbour integration points, as we can see in the following equation:

$$\overline{\boldsymbol{\varepsilon}} = \boldsymbol{\varepsilon} - \frac{1}{d} tr(\boldsymbol{\varepsilon})\mathbf{I} + \frac{1}{d}\overline{[tr(\boldsymbol{\varepsilon})]}^{p}\mathbf{I}, \tag{22}$$

where d is the dimension of the problem, in this case 3; and $\overline{[tr(\boldsymbol{\varepsilon})]}^{p}$ is the average trace of $\boldsymbol{\varepsilon}$ of the neighbour integration points in a chosen patch, calculated by:

$$\overline{[tr(\boldsymbol{\varepsilon})]}^{p} = \sum_{i=1}^{Nb} tr[\boldsymbol{\varepsilon}^{(i)}]\, w_i. \tag{23}$$

In addition, the trace could be obtained from the strain vector as:

$$\varepsilon_x + \varepsilon_y = \begin{bmatrix} 1 & 1 & 1 & 0 \end{bmatrix} \begin{bmatrix} \varepsilon_r \\ \varepsilon_z \\ \varepsilon_\theta \\ \gamma_{rz} \end{bmatrix} = \varepsilon_{kk} = m_k \varepsilon_k. \tag{24}$$

Rearranging the above equation using the B-matrix,

$$\varepsilon_{ll} = m_l \varepsilon_l = m_l B_{lk} u_k^h = T_k\, u_k^h, \tag{25}$$

where

$$T = \left[\tfrac{\partial N_1}{\partial r} + \tfrac{N_1}{r} \;\; \tfrac{\partial N_1}{\partial z} \,\middle|\, \tfrac{\partial N_2}{\partial r} + \tfrac{N_2}{r} \;\; \tfrac{\partial N_2}{\partial z} \,\middle|\, \cdots \right]. \tag{26}$$

Thus, the final lth-component of the tensor $\overline{\boldsymbol{\varepsilon}}$ (in Voigt form) for a single integration point i is calculated in the same way as in 2D problems:

$$\begin{aligned} \overline{\varepsilon}_l^{(i)} &= \left[B_{lk}^{(i)} - \frac{1}{d} m_l \left(T_k^{(i)} - \sum_{j=1}^{Nb} [T_k^{(j)} w^{(j)}] \right) \right] u_k^h \\ &= \overline{B}_{lk}^{(i)} u_k^h. \end{aligned}$$

2.3 B-Bar Implementation in $u - w$ Axisymmetric Problems

In order to apply the B-Bar method in a multiphase problem, we need to define a constitutive matrix first to relate stress with strain or displacements of the different phases. The proposed problem is the $u - w$ problem with soil and water phases. The effective stress tensor is calculated the same way as Eq. (7), if linear elasticity is assumed, the relationship between stresses and strains, expressed in its incremental form, is governed by Eq. (8), and p_w is obtained with the third Biot's equation:

$$\nabla \cdot d\dot{\boldsymbol{w}} + \boldsymbol{m}^T d\dot{\boldsymbol{\varepsilon}}^s + \frac{d\dot{p}_w}{Q} = 0$$

$$d\dot{p}_w = -Q\left[\nabla \cdot d\dot{\boldsymbol{w}} + \boldsymbol{m}^T d\dot{\boldsymbol{\varepsilon}}^s\right]$$

The final stress equation will be:

$$\boldsymbol{\sigma} = \boldsymbol{D}^e\ \boldsymbol{\varepsilon}^s + Q\left[tr(\boldsymbol{\varepsilon}^s) + tr(\boldsymbol{\varepsilon}^w)\right]\mathbf{I}.$$

If:

$$\boldsymbol{\varepsilon} = \begin{bmatrix} \varepsilon^s \\ \\ \varepsilon^w \end{bmatrix} = \begin{bmatrix} \varepsilon_r^s \\ \varepsilon_z^s \\ \varepsilon_\theta^s \\ \gamma_{rz}^s \\ \varepsilon_r^w \\ \varepsilon_z^w \\ \varepsilon_\theta^w \end{bmatrix} = \boldsymbol{S}\,\boldsymbol{u}$$

where $\boldsymbol{S}$ is the derivative matrix operator and $\boldsymbol{u}$ is a vector of displacements of both phases:

$$\begin{bmatrix} \varepsilon_r^s \\ \varepsilon_z^s \\ \varepsilon_\theta^s \\ \gamma_{rz}^s \\ \varepsilon_r^w \\ \varepsilon_z^w \\ \varepsilon_\theta^w \end{bmatrix} = \begin{bmatrix} \frac{\partial}{\partial r} & 0 & 0 & 0 \\ 0 & \frac{\partial}{\partial z} & 0 & 0 \\ \frac{1}{r} & 0 & 0 & 0 \\ \frac{\partial}{\partial z} & \frac{\partial}{\partial r} & 0 & 0 \\ 0 & 0 & \frac{\partial}{\partial r} & 0 \\ 0 & 0 & 0 & \frac{\partial}{\partial z} \\ 0 & 0 & \frac{1}{r} & 0 \end{bmatrix} \begin{bmatrix} u_r \\ u_z \\ w_r \\ w_z \end{bmatrix}.$$

In addition, the summation of traces of strain could be done with a $\boldsymbol{m}^*$ operator:

$$tr(\boldsymbol{\varepsilon}^s) + tr(\boldsymbol{\varepsilon}^w) = \boldsymbol{m}^T\boldsymbol{\varepsilon} = \begin{bmatrix}1&1&1&0&1&1&1\end{bmatrix}\begin{bmatrix}\varepsilon_r^s\\ \varepsilon_z^s\\ \varepsilon_\theta^s\\ \gamma_{rz}^s\\ \varepsilon_r^w\\ \varepsilon_z^w\\ \varepsilon_\theta^w\end{bmatrix}.$$

Thus, in Voigt notation:

$$\boldsymbol{\sigma} = \boldsymbol{D}^{e*}\,\boldsymbol{\varepsilon} + Q\,\boldsymbol{m}^T\boldsymbol{\varepsilon}\;\; \boldsymbol{m} = (\boldsymbol{D}^{e*} + Q\,\boldsymbol{m}^T\boldsymbol{m})\,\boldsymbol{\varepsilon} = \boldsymbol{D}^{u-w}\,\boldsymbol{\varepsilon}$$
$$= \begin{bmatrix}\frac{\lambda(1-\nu)}{\nu}+Q & \lambda+Q & \lambda+Q & 0 & Q & Q & Q\\ \lambda+Q & \frac{\lambda(1-\nu)}{\nu}+Q & \lambda+Q & 0 & Q & Q & Q\\ \lambda+Q & \lambda+Q & \frac{\lambda(1-\nu)}{\nu}+Q & 0 & Q & Q & Q\\ 0 & 0 & 0 & \mu & 0 & 0 & 0\\ Q & Q & Q & 0 & Q & Q & Q\\ Q & Q & Q & 0 & Q & Q & Q\\ Q & Q & Q & 0 & Q & Q & Q\end{bmatrix}\begin{bmatrix}\varepsilon_r^s\\ \varepsilon_z^s\\ \varepsilon_\theta^s\\ \gamma_{rz}^s\\ \varepsilon_r^w\\ \varepsilon_z^w\\ \varepsilon_\theta^w\end{bmatrix}.$$

If the problem needs a B-Bar based algorithm, it is necessary to calculate the average value of $\boldsymbol{\varepsilon}$. Thus, the main equation yields:

$$\overline{\boldsymbol{\varepsilon}} = \boldsymbol{\varepsilon} - \frac{1}{d}tr(\boldsymbol{\varepsilon}^s)\mathbf{I} + \frac{1}{d}[tr(\boldsymbol{\varepsilon}^s)]^p\mathbf{I} - \frac{1}{d}tr(\boldsymbol{\varepsilon}^w)\mathbf{I} + \frac{1}{d}[tr(\boldsymbol{\varepsilon}^w)]^p\mathbf{I}.$$

In Voigt notation the equation, the lth-component of the strain tensor is:

$$\overline{\varepsilon_l} = \varepsilon_l + \frac{1}{d}\left(-\varepsilon_{kk}\,m_l^s + \sum_{j=1}^{Nb}[\varepsilon_{kk}^{(j)}w^{(j)}]\,m_l^s - \varepsilon_{kk}^w\,m_l^w + \sum_{j=1}^{Nb}[\varepsilon_{kk}^{w(j)}w^{(j)}]\,m_l^w\right),$$

where

$$\varepsilon_{kk}^s = m_k^s\,\varepsilon_k = \begin{bmatrix}1&1&1&0&0&0&0\end{bmatrix}\begin{bmatrix}\varepsilon_r^s\\ \varepsilon_z^s\\ \varepsilon_\theta^s\\ \gamma_{rz}^s\\ \varepsilon_r^w\\ \varepsilon_z^w\\ \varepsilon_\theta^w\end{bmatrix},\ \varepsilon_{kk}^w = m_k^w\,\varepsilon_k = \begin{bmatrix}0&0&0&0&1&1&1\end{bmatrix}\begin{bmatrix}\varepsilon_r^s\\ \varepsilon_z^s\\ \varepsilon_\theta^s\\ \gamma_{rz}^s\\ \varepsilon_r^w\\ \varepsilon_z^w\\ \varepsilon_\theta^w\end{bmatrix}.$$

Additionally, we know that the strain tensor in Voigt notation is:

$$\varepsilon_l = S_{lj}u_j = S_{lj}N_{jk}u_k^h = B_{lk}u_k^h$$

where, in this case, yields:

$$\begin{bmatrix} \varepsilon_r \\ \varepsilon_z \\ \varepsilon_\theta \\ \gamma_{rz} \\ \varepsilon_r^w \\ \varepsilon_z^w \\ \varepsilon_\theta^w \end{bmatrix} = \left[\begin{array}{cccc|cccc} \frac{\partial N_1}{\partial r} & 0 & 0 & 0 & \frac{\partial N_2}{\partial r} & 0 & 0 & 0 \\ 0 & \frac{\partial N_1}{\partial z} & 0 & 0 & 0 & \frac{\partial N_2}{\partial z} & 0 & 0 \\ \frac{N_1}{r} & 0 & 0 & 0 & \frac{N_2}{r} & 0 & 0 & 0 \\ \frac{\partial N_1}{\partial z} & \frac{\partial N_1}{\partial r} & 0 & 0 & \frac{\partial N_2}{\partial z} & \frac{\partial N_2}{\partial r} & 0 & 0 \\ 0 & 0 & \frac{\partial N_1}{\partial r} & 0 & 0 & 0 & \frac{\partial N_2}{\partial r} & 0 \\ 0 & 0 & 0 & \frac{\partial N1}{\partial z} & 0 & 0 & 0 & \frac{\partial N_2}{\partial z} \\ 0 & 0 & \frac{N_1}{r} & 0 & 0 & 0 & \frac{N_2}{r} & 0 \end{array} \middle| \cdots \right] \begin{bmatrix} u_r^{(1)} \\ u_z^{(1)} \\ w_r^{(1)} \\ w_z^{(1)} \\ u_r^{(2)} \\ u_z^{(2)} \\ w_r^{(2)} \\ w_z^{(2)} \\ \vdots \end{bmatrix}.$$

In order to calculate ε_{ll}, the above equation can be rearranged as follows:

$$\begin{aligned} \varepsilon_{ll}^s &= m_l^s \varepsilon_l = m_l B_{lk}\, u_k^h = T_k^s\, u_k^h, \\ \varepsilon_{ll}^w &= m_l^w \varepsilon_l = m_l B_{lk}\, u_k^h = T_k^w\, u_k^h \end{aligned}$$

where

$$T^s = \left[\, \tfrac{\partial N_1}{\partial r} + \tfrac{N_1}{r}\ \tfrac{\partial N_1}{\partial z}\ 0\ 0 \middle| \tfrac{\partial N_2}{\partial r} + \tfrac{N_2}{r}\ \tfrac{\partial N_2}{\partial z}\ 0\ 0 \middle| \cdots \right],$$

$$T^w = \left[\, 0\ 0\ \tfrac{\partial N_1}{\partial r} + \tfrac{N_1}{r}\ \tfrac{\partial N_1}{\partial z} \middle| 0\ 0\ \tfrac{\partial N_2}{\partial r} + \tfrac{N_2}{r}\ \tfrac{\partial N_2}{\partial z} \middle| \cdots \right].$$

Thus, the final lth-component for the new strain tensor $\overline{\varepsilon}$ at a single integration point i in Voigt notation is calculated as:

$$\begin{aligned} \overline{\varepsilon_l}^{(i)} &= B_{lk}^{(i)} u_k^h - \frac{1}{d} m_l^s \left(T_k^{s(i)} u_k^h - \sum_{j=1}^{Nb} [T_k^{s(j)} w^{(j)}] u_k^h \right) \\ &\quad - \frac{1}{d} m_l^w \left(T_k^{w(i)} u_k^h - \sum_{j=1}^{Nb} [T_k^{w(j)} w^{(j)}] u_k^h \right) \\ &= \left[B_{lk}^{(i)} - \frac{1}{d} m_l^s \left(T_k^{s(i)} - \sum_{j=1}^{Nb} [T_k^{s(j)} w^{(j)}] \right) \right. \\ &\quad \left. - \frac{1}{d} m_i^w \left(T_k^{w(i)} - \sum_{j=1}^{Nb} [T_k^{w(j)} w^{(j)}] \right) \right] u_k^h \\ &\equiv \overline{B_{lk}}\, u_k^h. \end{aligned}$$

3 Application to Consolidation of Soils

As mentioned before, the settlement of saturated soils under loading is caused by a gradual interchange between pore pressure and effective stress. In this Section, we apply the above developed methodology for consolidation of soils at three different configurations: one dimensional case, radial consolidation and consolidation with sinks. Both static and dynamic scenarios are studied. The obtained solutions are compared with analytical or available numerical solutions.

3.1 Consolidation of a Column of Soil: Static, One Dimensional Case

In this case, the analytical solution for this problem is available, and thus it is compared with the solution proposed by the present method. Although the analytical solution is presented in non-dimensional terms, the geometry of the problem carried out is shown in Fig. 1. It consists of a column of 30 m of soil resting on an impermeable rigid base layer and loaded by a vertical, homogeneous loading at the top. The lateral displacements are restricted for both the solid and fluid phase. At the base layer, the solid phase is fixed, whereas the vertical movement of the fluid phase is

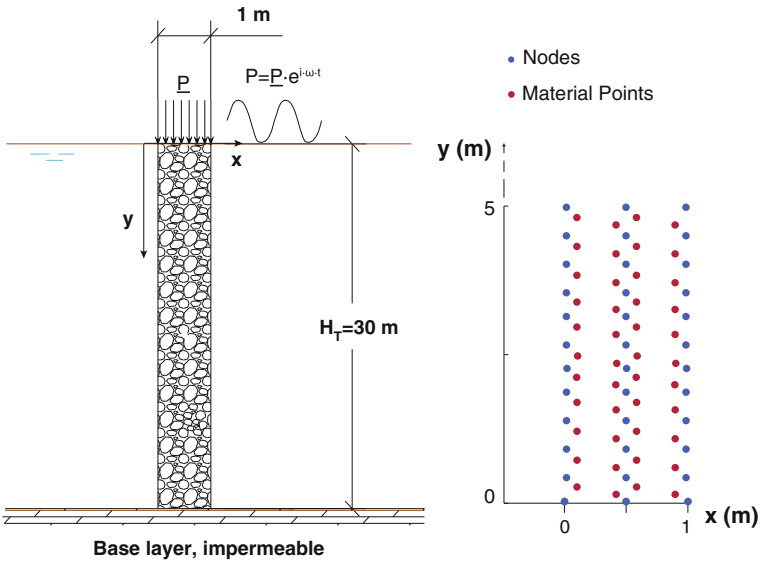

Fig. 1 Geometry, loading condition of the consolidation column, and the discretised nodes and material points (shown for the first 5 m only). The same geometry has been employed for both static and dynamic simulations

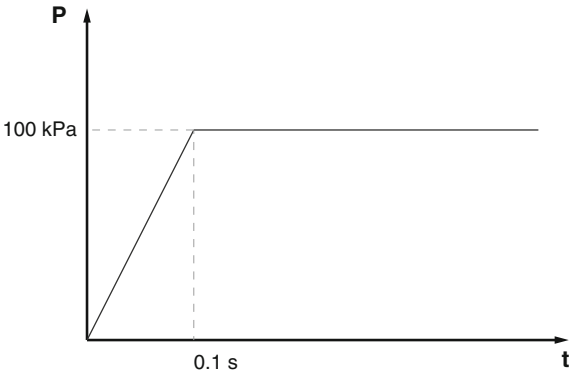

Fig. 2 Loading history in a monotonic problem

prevented. The column is discretised into 240 nodes and 183 material points. The external loading, in this case, is static at the end, but gradually applied as depicted in Fig. 2. The behaviour of the consolidation is led by the vertical consolidation coefficient, c_v, which is function of the vertical permeability coefficient, k_v:

$$c_v = \frac{k_v(1+e)}{\rho_w g a_v} = \frac{k_v}{\rho_w g} E_m = \frac{k_v}{\rho_w g m_v} \tag{27}$$

where a_v is the compressibility coefficient and m_v is the volumetric compressibility coefficient. The porous index, e, a measure of the porosity is expressed as follows:

$$e = \frac{n}{1-n}. \tag{28}$$

In Eq. (27), E_m is the oedometric modulus, related with the Young's modulus E according to the following equation:

$$E = E_m \left(1 - \frac{2\nu^2}{1-\nu}\right). \tag{29}$$

Typical values adopted for clays are 2 MPa for the Young's modulus and 0.33 for the Poisson's ratio.

The basic equation for one-dimensional consolidation derived by Terzaghi in 1923 [23] is

$$c_v \frac{\partial^2 \overline{u}}{\partial z^2} = \frac{\partial \overline{u}}{\partial t}. \tag{30}$$

The solution searched is a measure of the consolidation of the soil. It depends on the vertical time factor, T_v, defined by:

$$T_v = \frac{c_v t}{H^2}. \tag{31}$$

Adopting the degree of interstitial pressure dissipation, U_v, we can compare the analytical solution, given by the following equation, with the results obtained with the present research:

$$U_v(z) = 1 - \frac{u_e(z)}{u_{0e}} = 1 - \sum_{m=0}^{m=\infty} \frac{2}{M} \sin\left[M\left(1 - \frac{z}{H}\right)\right] \exp(-M^2 T_v) \tag{32}$$

where

$$M = \frac{\pi}{2}(2m+1), \quad m = 0, 1, 2, \ldots, \infty. \tag{33}$$

In Fig. 3, it is given the comparison between the analytical and the numerical solution along the depth of the column of soil for different values of T_v. As it is seen, all the values for T_v are dimensionless. With this comparison, we consider the current model employed is sufficiently validated.

This solution has been also compared with PLAXIS, in order to have an idea on the accuracy of this commercial software, since it is going to be employed hereinafter for several other theoretical examples. The direct conclusion obtained in Fig. 4 is that the accuracy decreases at the final stages of the consolidation. For low values of T_v PLAXIS solution of U_v along the column of soil is similar to the calculated

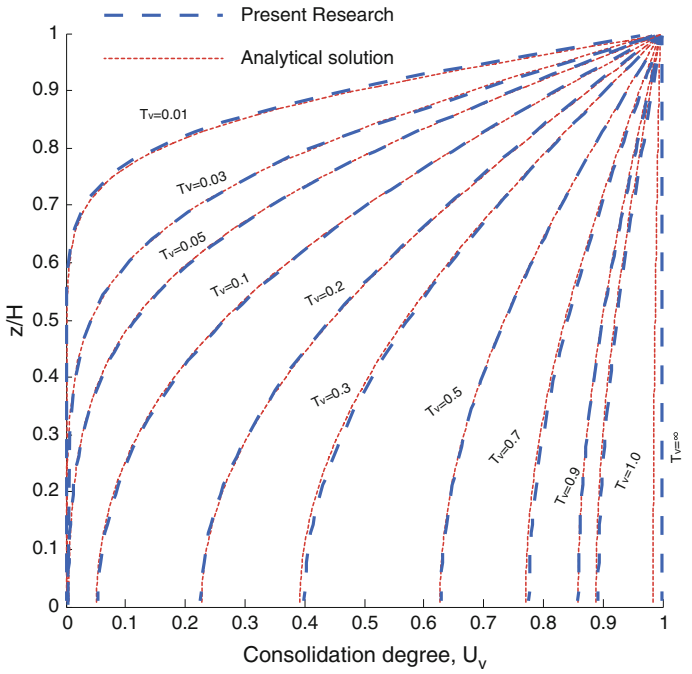

Fig. 3 Analytical and computational solution of U_v for different values of T_v

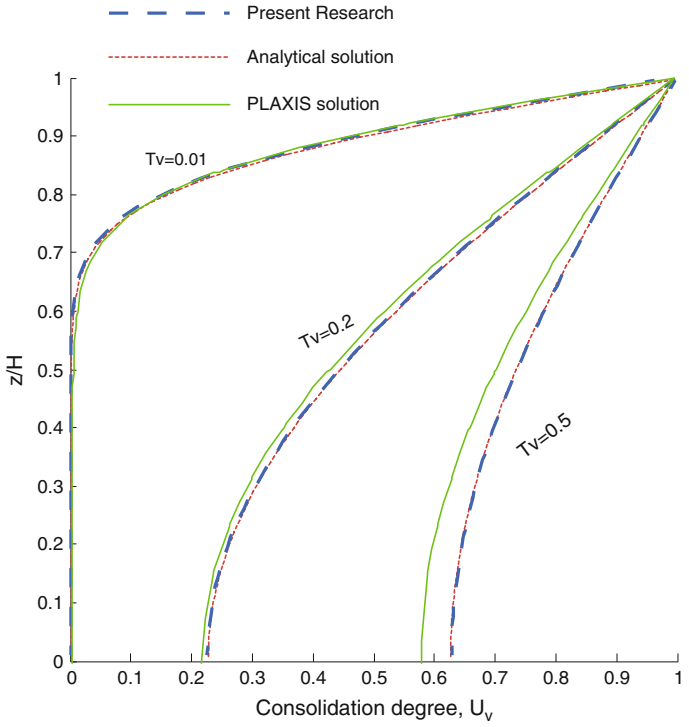

Fig. 4 Solutions of U_v for several values of T_v obtained in the current work compared with the analytical ones and those obtained with PLAXIS software

in this research, but is getting noticebly different for higher values of T_v. Therefore, PLAXIS solutions will provide a good approach of the trend of the pressure along the consolidation without an accurate degree of precision, at least, for one dimensional, static problems.

The solution for the monotonic loading at the upper side of the column shows the dissipation of the pore pressure along time. Figure 5 provides the comparison between the solution obtained with the present methodology, the $u - w$ solution obtained with a quadratic FEM model, and the one calculated using the software GeHoMadrid [25]. Hardly any perceptible difference can be noticed from these three solutions.

3.2 Consolidation of a Column of Soil: Dynamic, 1D Case

In this example, using the same geometry for the soil column, the consolidation of a soil column vertically subjected to harmonic pressure is obtained. This problem was first analytically solved by Zienkiewicz et al. [3] in 1980s, and recently by López-

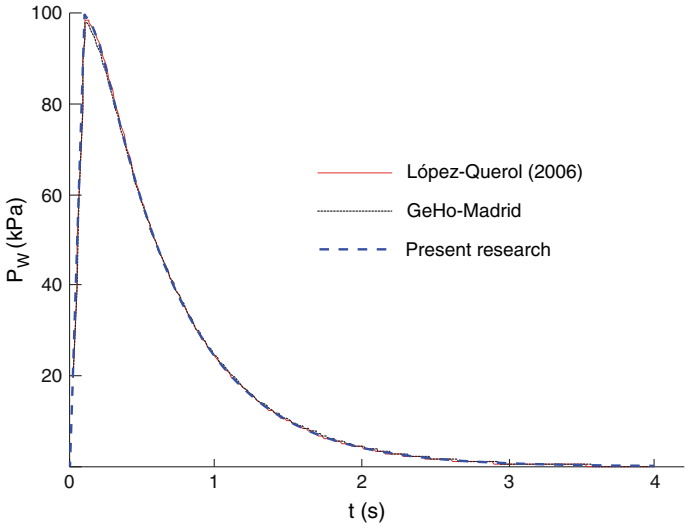

Fig. 5 Pore pressure evolution solutions at the *top* of the consolidation column

Table 1 Material parameters employed for the dynamic consolidation problem of a soil column

G (MPa)	ν (–)	n (–)	ρ (kg/m^3)	ρ_f (kg/m^3)	K_f (MPa)	ω (rad/s)	K_s (MPa)
312.5	0.2	0.333	3003	1000	10^3	3.379	10^{34}

Querol [26], among others, through employing quadratic finite element method. The parameters for the material are those presented in Table 1, where ω, is the applied loading frequency. A periodic surface load with the amplitude of 100 kPa, a frequency of 3.379 rad/s, is imposed. This dynamic load as well as all the material properties in Table 1 are chosen to be the same as those of Zienkiewicz et al. [3].

The variation of the pore pressure with depth is illustrated for different values of π_1, a dimensionless parameter defined as follows,

$$\pi_1 = k \frac{V_c^2}{g \, \frac{\rho_f}{\rho} \, \omega \, H_T^2}, \tag{34}$$

where H_T is the column height and V_c is the compressive wave velocity calculated as:

$$V_c = \sqrt{\left[D + \frac{K_f}{n} \right] \frac{1}{\rho}}, \quad D = \frac{2G(1-\nu)}{1-2\nu}, \tag{35}$$

where D the bulk modulus of the soil skeleton (dry mixture). Note that, for the given material properties and loading frequency, π_1 is proportional to the hydraulic conductivity k. Once k (thus π_1) is known, transient calculations can be carried out to obtain the envelop of the pore pressure history for different points along the column depth, or the isochrone.

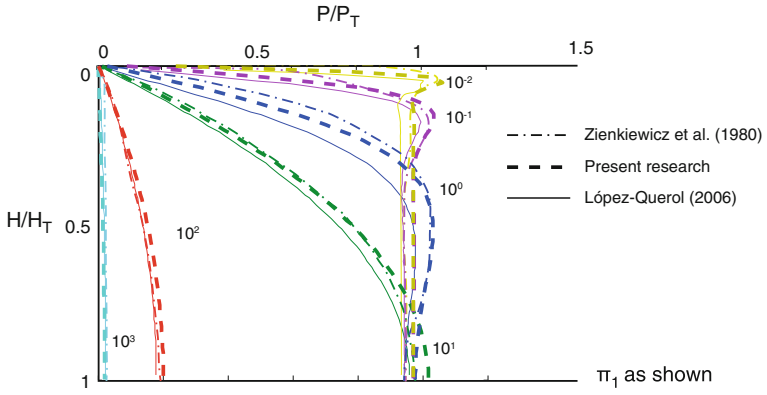

Fig. 6 Isochrones of the pressure in the whole column for different π_1 values: comparison for solutions taken from Zienkiewicz et al. [3], López-Querol [26] and those obtained in the present research. The depth is normalised by the column height, H_T, whereas the pore pressure is made non-dimensional by P_T, 100 kPa

After performing six different calculations for six different levels of π_1, from 10^{-2} to 10^3, we obtain the isochrones of the pore pressure depicted in Fig. 6. Additionally plotted are the results obtained by López-Querol [26] using quadratic finite elements formulating the problem in displacements as well, along with the analytical solutions provided by Zienkiewicz et al. [3]. It is noteworthy that the three different approaches achieve quite similar isochrone maps; nevertheless, whenever more scattering is observed, the current meshfree solution is closer to the analytical one.

3.3 Radial Consolidation: Static Axisymmetric Problems

The second problem carried out in this research is about radial consolidation. The physical equation which governs this problem is different from the Terzaghi's equation [23] shown in the previous section, i.e.:

$$c_h \left(\frac{\partial^2 u_r}{\partial r^2} + \frac{1}{r} \frac{\partial u_r}{\partial r} \right) = \frac{\partial u_r}{\partial t}, \tag{36}$$

where c_h is the horizontal consolidation coefficient, equivalent to the c_v coefficient in vertical consolidation:

$$c_h = \frac{k_h(1+e)}{\rho_w g a_v}. \tag{37}$$

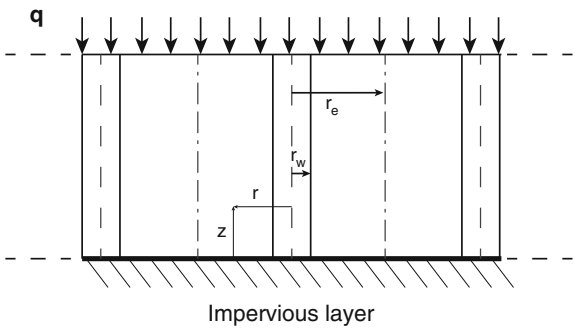

Fig. 7 Scheme of section of set of drains

In Fig. 7, a scheme of drains with induced radial flux is shown, where r and z directions are defined as depicted. There is an analytical solution for this problem given by Barron in 1948 [27] who defined the radial consolidation degree as a function of the non-dimensional time T_r:

$$U_r(T_r) = 1 - \exp\left[-\frac{2T_r}{F(n_r)}\right], \tag{38}$$

where

$$F(n_r) = \frac{n_r^2}{n_r^2 - 1}\log(n_r) - \frac{3n_r^2 - 1}{4n_r^2}. \tag{39}$$

The coefficient n_r depends on the relative extension of the drain in a particular geometry, for the section defined in Fig. 7, it is calculated as

$$n_r = \frac{r_e}{r_w}. \tag{40}$$

where r_w is the drain radius and r_e is the radius of influence for each type of problem. In this case a quadrangular net of drains shown in the scheme of Fig. 8 is studied.

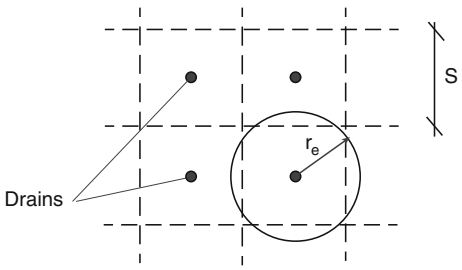

Fig. 8 Quadrangular net of drains ($r_e = 0.564\,S$)

Since radial consolidation equation involves a second term (tangential flow), it is not possible to solve within a plane strain formulation, as the one employed for vertical, one dimensional consolidation. Therefore, the axisymmetric framework, shown in previous sections, is employed instead and excellent results are obtained. In Fig. 9, several solutions of the radial consolidation degree, U_r, along the non-dimensional time T_r are shown. In addition, a comparison with a commercial software, PLAXIS, is given, even though this program does not allow us to implement a perfect radial consolidation due to the impossibility to neglect the vertical displacement throughout the domain. Two alternatives are proposed instead of the original problem, allowing for the vertical displacement: one assumes an impervious boundary condition on the top layer; the other one allows the flux of water through this boundary. Results in Fig. 10 offer a good trend in both cases but not the accuracy expected, as it occurs in the vertical consolidation too.

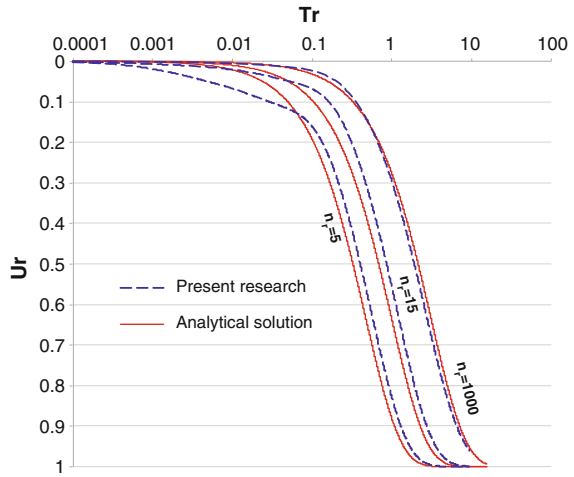

Fig. 9 Analytical and computational solutions of U_r along the non-dimensional time T_r

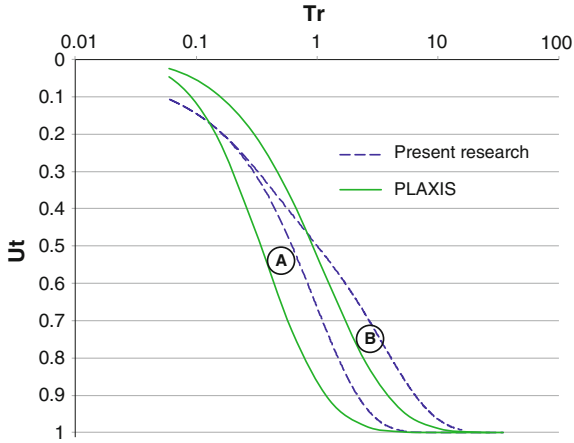

Fig. 10 Comparison between PLAXIS and present research solutions of $U_t = U_r + U_v$ along the non-dimensional time T_r for case A (permeable boundary) and B (impervious boundary)

3.4 Radial Consolidation: Dynamic Axisymmetric Problems

A dynamic loading on the surface has been applied, aiming to simulate its effect on the development of excess pore water pressure in the domain. The frequency of loading is the same as for the case of the soil column, while the amplitude is 50 kN. The geometry is the same as represented in Fig. 7. Vertical displacements of water in the entire domain have been prevented. Figure 11 represents the evolution of pore water pressure at the lateral, lowest corner, which clearly demonstrates the cyclic response of this result as well. From this figure it can be concluded that the generation and dissipation of excess pore water pressure are balanced in every cycle, and steady state is achieved from the very beginning of the loading. Additionally, Fig. 12 represents

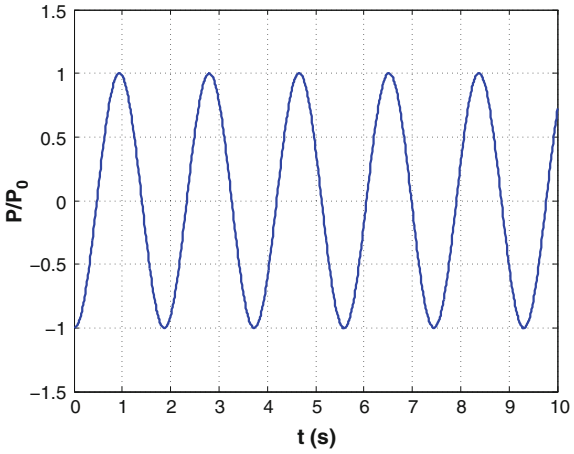

Fig. 11 Evolution of normalised excess pore water pressure during external cyclic loading (for the dynamic, radial consolidation problem)

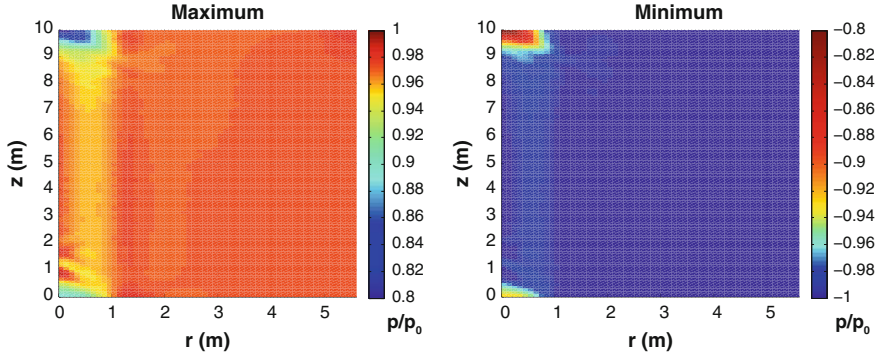

Fig. 12 Maximum and minimum normalised excess pore water pressures in dynamic, radial consolidation

maximum and minimum values of excess pore water pressure in the entire domain during the cyclic loading. This figure demonstrates the 2D nature of the problem, the drain being clearly displayed on the left hand side of the domain. Higher excess pore water pressures can be seen at the lower, left corner for both maximum and minimum cases. Moreover, the figure demonstrates the alternate positive and negative values for the pressures in the domain, as in Fig. 11.

3.5 Static Consolidation in a Soil with a Singular Point: Sink

The insertion of singular points inside the domain may vary the consolidation behaviour. The existence of a sink in the middle of horizontal soil layer is expected to accelerate the consolidation of the porous media, since this means an output of water at the permeable top boundary. To reproduce the sink, excess pore water pressure is not allowed to develop in several nodes in the centre of the domain (see Fig. 13). A square with one meter edge length is proposed for the study of this problem. Material properties are given in Table 2. Figures 14 and 15 show the comparison of results obtained with the present model as well as with PLAXIS for point (0, 0). Figure 14 provides the evolution in time of the degree of consolidation, U, at one of the corners at the bottom of the domain, whereas Fig. 15 represents the solutions in the whole domain after two seconds. In spite of slight differences in the final part of the evolution, it can be concluded that both results are fairly similar, demonstrating the good performance of the present formulation for this kind of problems.

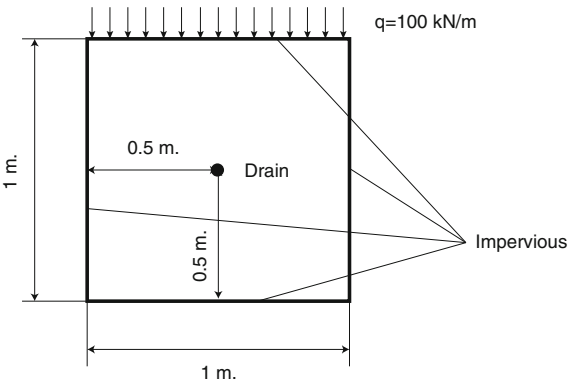

Fig. 13 Geometry for the problem of the sink

Table 2 Material parameters employed for the consolidation problem of a soil with a sink

E (MPa)	ν (–)	n (–)	ρ (kg/m^3)	ρ_f (kg/m^3)	K_f (MPa)	K_s (MPa)	k (m/s)	k_{sink} (m/s)
100	0.0	0.333	3003	1000	10^3	10^{34}	10^{-3}	10

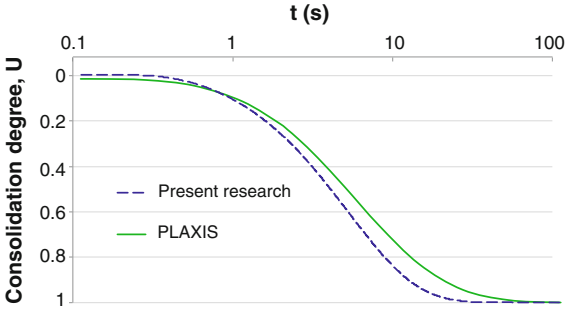

Fig. 14 Evolution of consolidation degree at the *bottom* corner for the sink problem. Present model versus PLAXIS

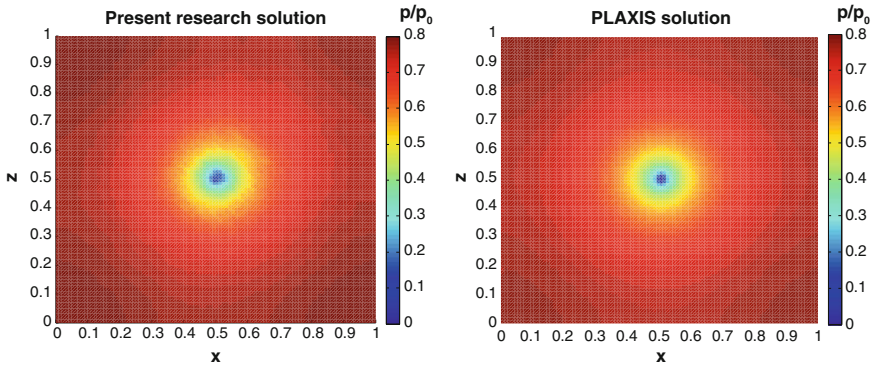

Fig. 15 Field of consolidation degrees in the domain after 2 s. Present model versus PLAXIS

3.6 Dynamic Consolidation in a Soil with a Singular Point: Sink

As for the case of radial consolidation, a dynamic simulation has been carried out. The geometry is the same as in Fig. 13. Figure 16 represents the evolution of normalised excess pore water pressure at a bottom corner, clearly showing the cyclic nature of the solution, which is steady from the beginning. Moreover, Fig. 17 shows maximum and minimum values in the whole domain. This figure clearly demonstrates the location of the sink, with zero water pressures in the centre of the domain for both cases. The alternate positive and negative values are also clear from the plot. Once again, these results demonstrate the suitability of the present formulation for dynamic consolidation problems in saturated soils.

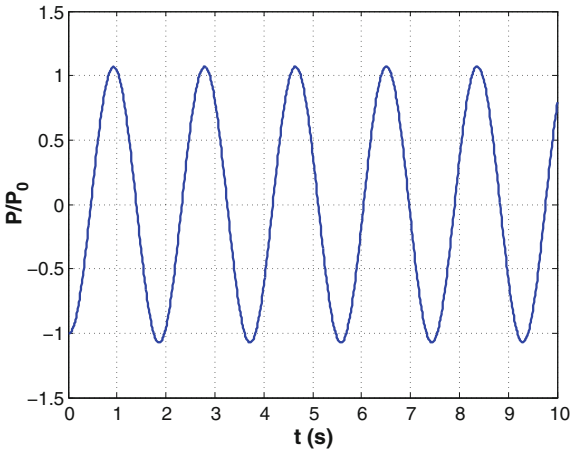

Fig. 16 Evolution of normalised excess pore water pressure during external cyclic loading (dynamic consolidation in a soil with a sink)

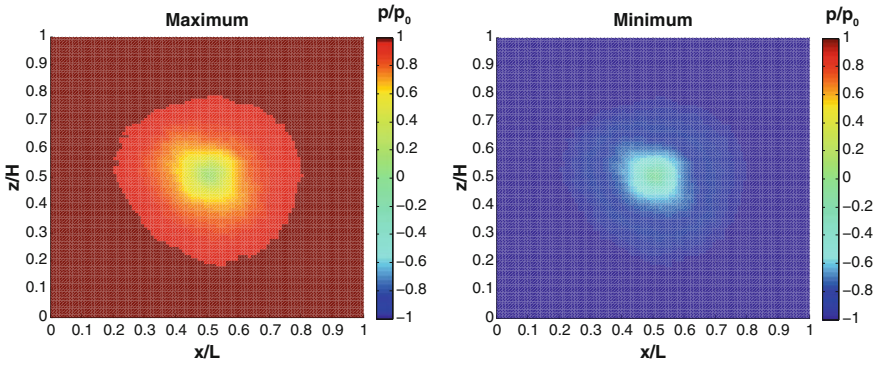

Fig. 17 Maximum and minimum normalised excess pore water pressures for dynamic soil consolidation with a sink

4 Conclusions

We have extended the previously developed B-bar based algorithm to meshfree numerical schemes in axisymmetric framework for both elastic and porous media. The methodology is applied to both static and dynamic consolidation problems in saturated soils. In particular, static and dynamic consolidation of a soil column, static and dynamic radial consolidation, static and dynamic consolidation with singular points (sinks), are carried out and compared with analytical solutions (whenever exist) or available finite element solutions. The feasibility of the current formulation in solving consolidation problems in saturated soils has been clearly demonstrated.

Acknowledgments This research has been partially funded by the Spanish Ministry of Economy and Competitiveness through the projects *BIA2012–31678* and *MAT2012–35416*. The first author also acknowledges the financial support via the fellowship No. *BES2013–063924*.

References

1. Biot, M. A. (1941). General theory of three-dimensional consolidation. *Journal of Applied Physics*, *12*(2), 155–164.
2. Biot, M. A. (1956). General solutions of the equations of elasticity and consolidation for a porous material. *Journal of Applied Mechanics*, 91–96.
3. Zienkiewicz, O. C., Chang, C. T., & Bettes, P. (1980). Drained, undrained, consolidating and dynamic behaviour assumptions in soils. *Géotechnique*, *30*(4), 385–395.
4. López-Querol, S., & Blazquez, R. (2006). Liquefaction and cyclic mobility model in saturated granular media. *International Journal for Numerical and Analytical Methods in Geomechanics*, *30*, 413–439.
5. Cividini, A., & Gioda, G. (2013). On the dynamic analysis of two-phase soils. In S. Pietruszczak & G. N. Pande (Eds.), *Proceedings of the third international symposium on computational geomechanics (ComGeo III)* (pp. 452–461).
6. Ortiz, A., Puso, M. A., & Sukumar, N. (2004). Construction of polygonal interpolants: A maximum entropy approach. *International Journal for Numerical Methods in Engineering*, *61*(12), 2159–2181.
7. Arroyo, M., & Ortiz, M. (2006). Local maximum-entropy approximation schemes: A seamless bridge between finite elements and meshfree methods. *International Journal for Numerical Methods in Engineering*, *65*(13), 2167–2202.
8. Li, B., Habbal, F., & Ortiz, M. (2010). Optimal transportation meshfree approximation schemes for fluid and plastic flows. *International Journal for Numerical Methods in Engineering*, *83*, 1541–1579.
9. Nelder, J. A., & Mead, R. (1965). A simplex method for function minimization. *Computer Journal*, *7*, 308–313.
10. Hughes, T. J. R. (1980). Generalization of selective integration procedures to anisotropic and nonlinear media. *International Journal for Numerical Methods in Engineering*, *15*, 1413–1418.
11. Simo, J. C., & Rifai, M. S. (1990). A class of mixed assumed strain methods and the method of incompatible modes. *International Journal for Numerical Methods in Engineering*, *29*, 1595–1638.
12. Kasper, E. P., & Taylor, R. L. (2000). A mixed-enhanced strain method: Part I: Geometrically linear problems. *Computers and Structures*, *75*(3), 237–250.
13. De Souza Neto, E. A., Pires, F. M., & Owen, D. R. J. (1980). F-bar-based linear triangles and tetrahedra for finte strain analysis of nearly incompressible solids. Part I: Formulation and benchmarking. *International Journal for Numerical Methods in Engineering*, *62*, 353–383.
14. Bonet, J., & Burton, A. J. (1998). A simple average nodal pressure tetrahedral element for incompressible and nearly incompressible dynamic Explicit applications. *Communications in Numerical Methods in Engineering*, *14*(5), 437–449.
15. Hauret, P., Kuhl, E., & Ortiz, M. (2007). Diamond elements: A finite element/discrete-mechanics approximation scheme with guaranteed optimal convergene in incompressible elasticity. *International Journal for Numerical Methods in Engineering*, *73*, 253–294.
16. Elguedj, T., Bazilevs, Y., Calo, V. M., & Hughes, T. J. R. (2008). $\overline{B}$ and $\overline{F}$ projection methods for nearly incompressible linear and non-linear elasticity and plasticity using higher-order NURBS elements. *Computer Methods in Applied Mechanics and Engineering*, *197*(33–40), 2732–2762.
17. Artioli, E., Castellazzi, G., & Krysl, P. (2014). Assumed strain nodally integrated hexahedral finite element formulations for elastoplastic applications. *International Journal for Numerical Methods in Engineering*, *99*(11), 844–866.

18. Ortiz, A., Puso, M. A., & Sukumar, N. (2010). Maximum-entropy meshfree method for compressible and near-incompressible elasticity. *Computer Methods in Applied Mechanics and Engineering*, *199*, 1859–1871.
19. Navas, P., López-Querol, S., Yu, R. C., & Li, B. (2016). B-bar based algorithm applied to meshfree numerical schemes to solve unconfined seepage problems through porous media. *International Journal for Numerical and Analytical Methods in Geomechanics*, *40*, 962–984.
20. López-Querol, S., Navas, P., Peco, J., & Arias-Trujillo, J. (2011). Changing impermeability boundary conditions to obtain free surfaces in unconfined seepage problems. *Canadian Geotechnical Journal*, *48*, 841–845.
21. Navas, P., & López-Querol, S. (2013). Generalized unconfined seepage flow model using displacement based formulation. *Engineering Geology*, *166*, 140–141.
22. Biot, M. A. (1956). Theory of propagation of elastic waves in a fluid-saturated porous solid. I. Low-Frequency range. *Journal of the Acoustical Society of America*, *28*(2), 168–178.
23. Terzaghi, K. V. (1925). Principles of Soil Mechanics. *Engineering News-Record*, *95*, 19–27.
24. Zienkiewicz, O. C., & Taylor, R. L. (1994). *El método de los elementos finitos. Vol 1: Formulación básica y problemas lineales*. Barcelona: CIMNE.
25. Fernández Merodo, J. A., Mira, P., Pastor, M., & Li, T. (1999). *GeHoMadrid User Manual*. Madrid: CEDEX. Technical Report.
26. López-Querol, S. (2006). *Modelización geomecánica de los procesos de densificación, licuefacción y movilidad cíclica de suelos granulares sometidos a solicitaciones dinámicas*. PhD thesis, University of Castilla-La Mancha, Ciudad Real, Spain.
27. Barron, R. A. (1948). Consolidation of fine-grained soils by drain wells. *Transationc ASCE*, *113*, 718–754.